E-Z Isomerization in Guanidine: Second-order Saddle Dynamics, Non-statisticality, and Time-frequency Analysis

Richa Rashmi,[+,a] Pankaj Kumar Yadav,[+,a] Aniruddha Seal,[a] Manikandan Paranjothy*[b] Upakarasamy Lourderaj,*[a]

Our recent work on the $E-Z$ isomerization reaction of guanidine using *ab initio* chemical dynamics simulations [Richa et al, *Regul. Chaotic Dyn.* **2021**, *26*, 119] emphasized the role of second-order saddle (SOS) in the isomerization reaction; however could not unequivocally establish the non-statistical nature of the dynamics followed in the reaction. In the present study, we performed thousands on-the-fly trajectories using forces computed at the MNDO level to investigate the influence of second-order saddle in the $E-Z$ isomerization reaction of guanidine and the role of intramolecular vibrational energy redistribution (IVR) on the reaction dynamics. The simulations reveal that while majority of the trajectories follow the traditional transition state pathways, 15% of the trajectories follow the SOS path. The dynamics was found to be highly non-statistical with the survival probabilities of the reactants showing large deviations from those obtained within the RRKM assumptions. In addition, a detailed analysis of the dynamics using time-dependent frequencies and the frequency ratio spaces reveal the existence of multiple resonance junctions that indicate the existence of regular dynamics and long-lived quasi-periodic trajectories in the phase space associated with non-RRKM behavior.

1. Introduction

The concept of transition state (TS) and minimum energy path (MEP) are vital to understanding the mechanism of chemical reactions. The transition state is a first-order saddle point (index 1 saddle) on the potential energy surface (PES) of the system and it connects two associated minimum energy points (reactant/products/intermediates). However, different types of stationary points can exist on the PES of a system.[1] For a system consisting of N atoms, a stationary point on the PES is defined as an n^{th}-order saddle if it is a maximum along n orthogonal coordinates and a minimum along the rest of the $3N-6-n$ coordinates. In particular, second-order saddle (SOS) points on the PES have been identified in several systems. The ring-opening reaction of cyclobutene to 1,3-butadiene was observed to occur via a disrotatory pathway through an SOS, as opposed to the conrotatory pathway predicted based on the Woodward–Hoffman rules.[2] An SOS was also observed on the isomerization pathways of NH_5 and NF_2H_3.[3,4] A non-traditional trifurcation pathway was observed for S_N2 type reactions, $X^- + CH_4 \rightarrow XCH_3 + H^-$ (X = H, F) and $CN^- + CH_3F \rightarrow CNCH_3 + F^-$ due to the presence of a second-order saddle point on the MEP.[5] In addition, SOS have also been reported in the Diels-Alder reactions.[6] However, higher-order saddles are generally higher in energy than the transition states along the intrinsic reaction coordinate (IRC), and hence they were often considered insignificant in describing reaction pathways and ignored.

Recently, the investigation of the role of SOS on the reaction mechanisms and dynamics have gained attention. Ezra and Wiggins studied the role of SOS in chemical reactions examining the phase-space structures using two-dimensional (2D) model Hamiltonians.[7,8] Pradhan and Lourderaj found that the formation of cyclopropane in the thermal denitrogenation of 1-pyrazoline followed an SOS pathway in addition to the traditional TS pathways using *ab initio* classical trajectory (AICT) simulations.[9,10] They also found that increasing the total energy available to the system, increased the fraction of trajectories following the SOS pathway and led to competitive dynamical pathways.[11] Recently, Srihari and coworkers studied the influence of SOS on double proton transfer reactions performing classical and quantum dynamical simulations on a 2D model potential.[12]

In this context, it is of fundamental importance to understand the (non-)statisticality in the dynamics of the reaction, particularly following SOS pathways. The deviations from statisticality are associated with slow and incomplete intramolecular vibrational energy redistribution (IVR) during the dynamics. Hence, it is important to study the phase space structures of the system to identify the possible bottlenecks to IVR in the phase space. However, for multi-dimensional systems (greater than 3 degrees of freedom) understanding of the phase space structures is challenging, and time-frequency analysis in combination with identifying important frequency ratios between relevant modes have been used to study the IVR and the underlying higher-dimensional phase space.[13–18]

The studies reported above on the reactions with SOS on the PES illustrate the influence of SOS on the dynamical paths followed in the reactions and emphasize the need to

[a] R. Rashmi, Dr. P. K. Yadav, A. Seal, Prof. U. Lourderaj*
National Insitute of Science Education and Research (NISER) Bhubaneswar
An OCC of Homi Bhabha National Institute
P. O. Jatni, Khurdha, Odisha 752050 India
E-mail: u.lourderaj@niser.ac.in

[b] Prof. M. Paranjothy*
Department of Chemistry
Indian Institute of Technology Jodhpur
Jodhpur, Rajasthan, India
E-mail: pmanikandan@iitj.ac.in

[+] These authors contributed equally.

identify more systems where SOS dynamics are crucial. To this end, we recently studied the *E-Z* isomerization reaction of guanidine as a model system to understand the role of second-order saddle in isomerization reaction using AICT simulations at the MP2/6-31+G* level of theory.[19] The isomerization can occur via TSs or an SOS where the SOS is only about 1 kcal/mol higher in energy than the TS. We initiated trajectories from the reactant region, TS region, and SOS region and found that the isomerization happened via the transition states as well as the second-order saddle. The simulations indicated non-statistical dynamics with trajectories exhibiting recrossing and a 3% deviation from the RRKM rate constants. To further understand the non-statisticality, a wavelet-based time-frequency analysis was done to study the phase space structures and understand the role of IVR. This was carried out both on the time-evolved internal coordinates and the principal components extracted from principal component analysis (PCA)[20–22] performed on the intrinsic reaction coordinate (IRC). The frequencies thus extracted indicated regular dynamics and existence of long-lived quasi-periodic trajectories in the phase space. The frequency ratio space (FRS) showed localized regions or possible resonance junctions in the phase space. For a large-dimensional system like guanidine, any quantitative conclusion from the frequency ratio spaces would require a large ensemble of trajectories. However, AICT calculations at the MP2/6-31+G* level of theory are computationally demanding and are not practically feasible to compute thousands of trajectories integrated for long time scales of the order of 50 ps, which are necessary to produce statistically reliable data.

In the present study, we performed on-the-fly trajectory simulations using the forces computed at the MNDO level to investigate the role of second-order saddle in the *E-Z* isomerization reaction of guanidine. The semi-empirical Hamiltonian (MNDO) was chosen to reduce the computational cost and compute a large ensemble of trajectories. In section 2, the PES for the *E-Z* isomerization reaction of guanidine computed using different semi-empirical methods is discussed and compared with the *ab inito* (MP2) studies. In section 3, the dynamics of the isomerization, reaction pathways, reaction lifetimes, and RRKM rate constants are discussed. In section 4, the time-frequency analysis and the associated frequency ratio space are discussed. Finally, the important findings of the study are summarized in Conclusion.

2. Potential Energy Surface

Guanidine isomerizes from the *E* (**R**) to *Z* (**P**) isomer following a clockwise rotation about the imine C−N bond via the transition state **TS1**, or an anti-clockwise rotation via the transition state **TS2**. In addition, the isomerization is also possible by an in-plane wagging of the imine -NH group through a second-order saddle, **SOS** (Figure 1a). The isomerization reaction of guanidine was earlier studied by us at the MP2/6-31+G* level of theory.[19] However, as mentioned above, it is important to identify a semi-empirical Hamiltonian to compute a large ensemble of on-the-fly trajectories, due to their low computational cost. The semi-empirical method should reproduce the important features of the potential energy surface accurately as compared to that of *ab initio* methods. Different semi-empirical methods were tested to identify the stationary points on the potential energy surface. The stationary points were characterized by computing the harmonic frequencies. The calculations were carried out using the MOPAC-5.021mn software.[23] The energies and important mode frequencies for the stationary points obtained using the different semi-empirical methods are presented in Table S1 in the Supplementary Information (SI). We can see that among the methods used, MNDO and PM3 methods give energeties comparable to that of the MP2/6-31+G* level. The **TS2** and **SOS** MNDO energies are 3.17 and 2.75 kcal/mol higher than that of the MP2 values. The energy difference between the **TS2** and **SOS** is 0.56 kcal/mol which is comparable to the MP2 value of 0.98 kcal/mol. In the case of PM3, while the energies of the **TS2** and **SOS** are closer to that of MP2 values, the energy gap between **TS2** and **SOS** is 2.42 kcal/mol. Since, one of the aims of the present work is to understand the role of SOS as competing path to that of the TS paths, we chose MNDO method for further studies.

The potential energy profile for the *E-Z* isomerization of guanidine mapped using the MNDO Hamiltonian is shown in Figure 1a. A comparison of MNDO results (important geometrical parameters and harmonic mode frequencies) with that of MP2 is given in Table 1. A relaxed PES scan was performed with respect to the internal coordinates ϕ and α to construct the PES of guanidine isomerization using MOPAC-5.021mn software[23] where ϕ corresponds to the torsional $\angle$N2C1N3H5 and α corresponds to $180° - \angle$C1N3H5. The minimum energy pathways were confirmed from IRC calculations from **TS1**, **TS2**, and **SOS**. Figure 1b shows the polar plot representing the 2D PES for guanidine isomerization with the IRCs projected on it. The IRC calculations for the **R**→**TS1**→**P**, **R**→**TS2**→**P**, and **R**→**SOS**→**P** pathways were computed using a modified version of the VENUS[24,25]interfaced with MOPAC-5.021mn software.[23] The MEP along the **TS1**→**SOS**→**TS2** pathway was calculated by a constrained optimization.

3. Isomerization Dynamics

To investigate the *E-Z* isomerization dynamics of guanidine, a total of 5000 trajectories were initiated from the reactant region with the forces necessary for integration calculated on-the-fly using the MNDO Hamiltonian. The trajectories were integrated for 50 ps with a time step of 0.2 fs using the velocity-Verlet algorithm. The initial coordinates and momenta were chosen using the microcanonical normal mode sampling with the total energy computed as,

$$E_{\text{total}} = \Delta E + E_{\text{ZPE}} + E_{\text{vib}} + E_{\text{rot}} + 2RT \qquad (1)$$

Here, ΔE is the classical energy difference between reactant and **SOS**, E_{ZPE}, E_{vib}, and E_{rot} are the zero-point-energy, average vibrational energy, average rotational energy of **SOS** respectively, and RT is the energy along each of the two orthogonal coordinates with negative curvatures at 298.15 K. The total energy thus available to the system is 77.81 kcal/mol. The trajectories were calculated using a modified version of VENUS[?] interfaced with MOPAC-5.021mn software.[23] It is worth noting that the integration of a trajectory at the MNDO level for 2 ps takes about 3 minutes on a single core Intel Xeon processor compared to ∼24 hours on an 8 core Intel Xeon processor at the MP2/6-31+G* level of theory.

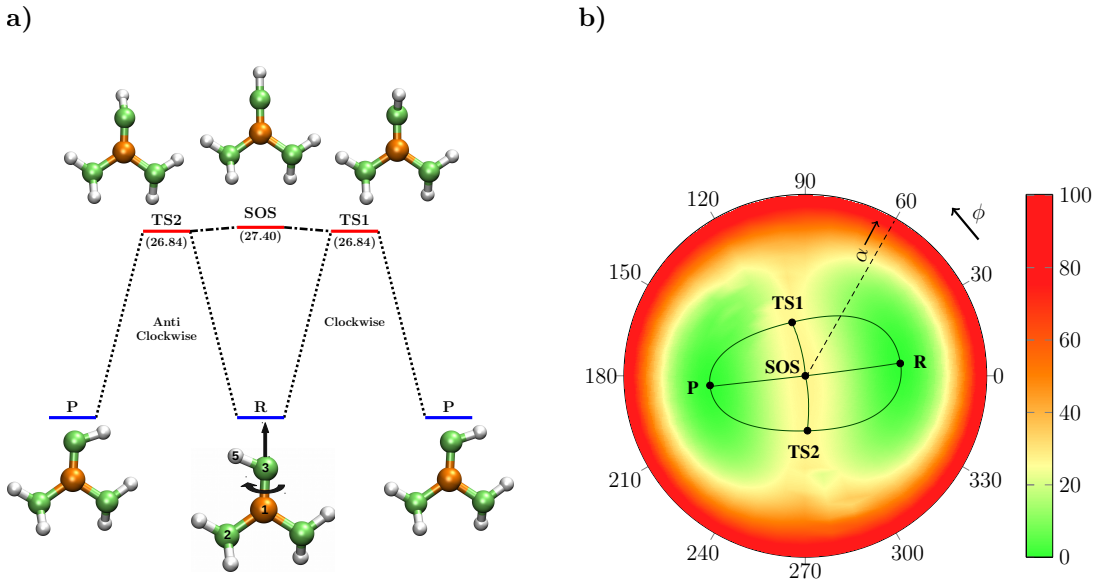

Figure 1. (a) Potential energy profile for the $E - Z$ isomerization of guanidine. (b) 2D PES for *E-Z* isomerization of guanidine using MNDO. The solid lines represent the projection of the IRC path on the PES. All energies are in kcal/mol and ϕ is in degrees.

Table 1. Comparison of MNDO results with MP2 results for guanidine isomerisation

Parameters	**R**		**SOS**		**TS2**	
	MP2	**MNDO**	**MP2**	**MNDO**	**MP2**	**MNDO**
Relative Energy (kcal/mol)	0.00	0.00	24.65	27.40	23.67	26.84
Geometry						
α_0 (°)	68.83	64.41	0.00	0.024	40.50	36.95
ϕ_0 (°)	8.54	7.43	-	-	272.69	272.27
N−H stretch (Å)	1.02	1.00	0.99	0.97	1.00	0.97
Frequencies (cm^{-1})						
In-plane mode	-	-	$1078i$	$1210i$	-	-
Out-of-plane mode	-	-	$368i$	$260i$	-	-
Torsional mode (ϕ)	847	823	-	-	$1031i$	$1204i$
C-N-H bend (α)	1151	1312	-	-	-	-
N-H stretch	3513	3576	-	-	-	-

3.1. Dynamical Pathways

To understand the dynamical pathways followed in the reaction, different regions on the PES were identified. Details of the definitions of the different regions are given in the SI (Section S2). The six stationary point regions (**R, TS1, TS2, SOS, PW, PM**) and a dividing surface thus identified on the 2D PES are given in Table S2 and shown in Figure 2. It should be noted that a trajectory, on crossing the dividing surface, enters the product well region (**PW**) and then either forms the product defined by the region around the product minimum (**PM**), or recrosses the dividing surface without reaching the **PM** region. Thus, the two regions **PW** and **PM** were differentiated to identify recrossing events. For the purpose of categorizing the trajectories as reactive (i.e. isomerization event), the trajectories were followed until the first instance of entry into the **PM** region.

Out of the 5000 trajectories initiated from the reactant region, 2248 were reactive, where the trajectories started from **R** and reached **PM** within the 50 ps of integration time. The rest of the trajectories were non-reactive and did not reach the **PM** region for the entire integration time. The dynamical pathways followed by the trajectories were classified by tracking the regions accessed by them before forming the products. Details of the classification of trajectories are given in SI. The various pathways followed by the 2248 reactive trajectories are shown in Table 2. We can see that the paths **R→TS1→PW→PM** and **R→TS2→PW→PM** are highly favoured with 942 trajectories following the path through **TS1** and 875 through **TS2**. The pathway **R→SOS →PW→PM** is about three times less favoured (269 trajectories). We see that trajectories also followed paths involving multiple saddle points including **SOS** region. In 58 trajectories (Paths 4 and 5), the system reaches **SOS** directly from the reactant and then bifurcates to **TS1** or **TS2** regions before forming products. Also, a fraction of trajectories reach the **SOS** region via **TS1** and **TS2** and

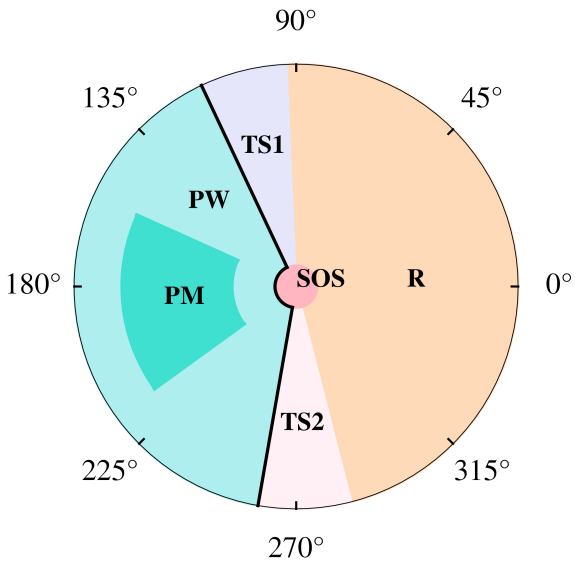

Figure 2. The definition of different stationary point regions on the PES and dividing surface (black solid line) marked on the 2D PES.

then form products (paths 6 and 7 respectively). A few trajectories, access all the three saddles, i.e. **TS1**, **SOS**, and **TS2** before forming products. It is important to note that 46 out of the 2248 reactive trajectories show recrossing events (paths 10-23) which evidences the non-statistical nature of the isomerization reaction. In addition, 26 of the non-reactive trajectories also showed recrossing behavior.

3.2. Non-statistical Dynamics

Non-statistical dynamics has been illustrated in several systems by experimental and computational studies.[11,26–30] To investigate the apparent non-statistical dynamics indicated by pathways followed in the trajectories, we computed the lifetime of the reaction for each reactive trajectory, which is the integration time until the reactive event (i.e. the first instance of entry into **PM** region). The criterion was chosen so that we can account for the recrossing dynamics (see above). Figure 3 shows the lifetime distribution for all the reactive trajectories. The average lifetimes for the trajectories forming the product from **SOS** (Paths 1, 6, 7, 10, 11, 22, and 23), **TS1** (Paths 2, 4, 8, 9, 12, 14, 15, 16, 19, and 21), and **TS2** (Paths 3, 5, 13, 17, 18, and 20) are 21.21, 22.92 and 22.14 ps respectively. It is of interest to compare these lifetimes with those obtained from statistical theories. To this end, we calculated RRKM rate constants[31] $k(E)$ for the paths **R→TS1→PM**, **R→TS2→PM**, and **R→SOS→PM** given by

$$k(E) = \frac{N^{\ddagger}(E - E_0)}{h\rho(E)} \qquad (2)$$

where E_0 is the relative energy of the saddle point, E is the energy available to the reactant, h is the Planck's constant, $N^{\ddagger}(E - E_0)$ is the sum of states for the saddle point, and $\rho(E)$ is the density of states for the reactant. However, it should be noted that the RRKM rate constant is not defined for a second-order saddle point since it corresponds to a stationary point with two imaginary frequencies. For guanidine, these correspond to an in-plane motion and an out-of-plane motion of the imine H atom. The rate constant $k_{\mathbf{SOS}}$ was computed using an approximate sum of states calculated by considering the absolute value of the imaginary frequency corresponding to the out-of-plane motion along with the other $(3N - 8)$ frequencies. Anharmonicity corrections to the sum and density of states were calculated by the method of Haarhoff.[32] The rate constants and the corresponding lifetimes thus obtained are reported in Table 3 and compared with those obtained from the MP2/6-31+G* PES. We can see that rate constants obtained from the MP2/6-31+G* PES for **TS1** and **TS2** are ∼1.5 times larger than those obtained from the MNDO PES, that can be possibly due to the higher energies of the TSs on the MNDO PES compared to that of the MP2 PES. Also, the MNDO $k_{\mathbf{SOS}}$ was found to be larger than $k_{\mathbf{TS1/TS2}}$ due to lower values of the sum of states for the TSs. The anharmonicity effects were not found to be significant here. Nevertheless, the lifetimes obtained from the RRKM (harmonic, MNDO) rate constants are 35.3, 35.1, and 25.1 ps for **TS1**, **TS2**, and **SOS** respectively indicating non-statistical dynamics followed in the reaction.

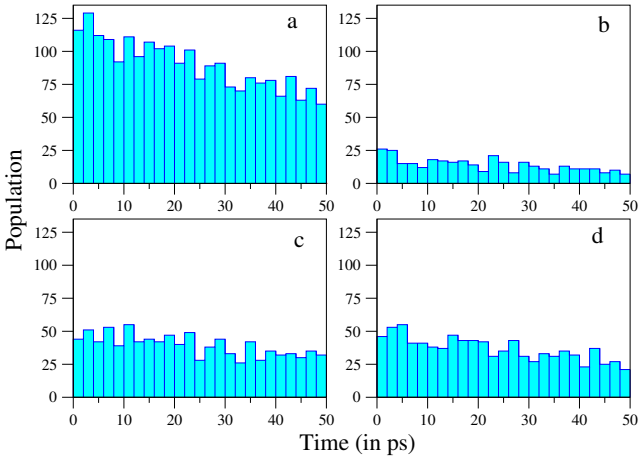

Figure 3. Reaction lifetime distribution for (a) all reactive trajectories, trajectories reaching **PM** from (b) **SOS**, (c) **TS1**, and (d) **TS2**.

To substantiate the non-statistical dynamics followed in the isomerization of guanidine, we computed the survival probability along each pathway from the fraction of the unreacted species $N(t)$ at time t obtained from trajectory simulations and compared with the distribution expected from RRKM theory.[33,34] The survival probability is given by

$$\frac{N(t)}{N(0)} = e^{-k(E)t} \qquad (3)$$

The survival probabilities from all the reactive trajectories and for the individual isomerization paths via **SOS**, **TS1**, and **TS2** are compared with their respective RRKM distributions in Figure 4. Clearly, the survival probability distributions from the trajectories exhibit a large deviation from the RRKM ones emphasizing the non-statistical nature of the isomerization dynamics.

4. Time-Frequency Analysis in a Reduced Dimensional Space

To understand the non-statisticality and the role of IVR in the isomerization reaction, it is essential to understand the phase space structures. Since, the phase space for the

Table 2. Various dynamical pathways followed by the 2248 reactive trajectories

Path No.	Pathway	No. of trajectories
1	**R→SOS→PW→PM**	269
2	**R→TS1→PW→PM**	942
3	**R→TS2→PW→PM**	875
4	**R→SOS→TS1→PW→PM**	29
5	**R→SOS→TS2→PW→PM**	29
6	**R→TS1→SOS→PW→PM**	16
7	**R→TS2→SOS→PW→PM**	39
8	**R→TS1→SOS→TS1→PW→PM**	2
9	**R→TS2→SOS→TS1→PW→PM**	1
	Recrossing trajectories	
10	**R→TS2→PW→SOS→PW→PM**	13
11	**R→TS1→PW→SOS→PW→PM**	8
12	**R→TS2→PW→TS2→R→TS1→PW→PM**	4
13	**R→TS2→PW→TS2→R→TS2→PW→PM**	5
14	**R→TS2→SOS→PW→TS1→PW→PM**	1
15	**R→TS2→PW→TS2→R→TS2→R→TS2→R→TS1→PW→PM**	2
16	**R→TS2→PW→TS2→R→SOS→R→TS1→PW→PM**	1
17	**R→TS2→PW→TS2→R→SOS→R→TS2→PW→PM**	3
18	**R→TS2→PW→TS2→PW→PM**	4
19	**R→TS2→PW→TS2→R→TS2→R→TS1→PW→PM**	1
20	**R→TS2→PW→TS2→R→TS2→R→TS2→PW→PM**	1
21	**R→TS2→PW→TS2→R→TS1→R→TS1→PW→PM**	1
22	**R→TS2→PW→TS2→R→TS2→R→TS2→SOS→R→SOS→PW→PM**	1
23	**R→TS2→PW→TS2→R→TS2→R→TS2→R→SOS→R→SOS→PW→PM**	1

Table 3. Harmonic and anharmonic RRKM rate constants for the three isomerization paths calculated using the frequencies obtained from the MNDO and MP2/6-31+G* levels of theory

S. No.	Paths	MNDO (s^{-1})		MP2 (s^{-1})
		Harmonic	Anharmonic	Harmonic
1	$k_{\mathbf{TS1}}$	2.83×10^{10}	2.32×10^{10}	4.58×10^{10}
2	$k_{\mathbf{TS2}}$	2.85×10^{10}	2.33×10^{10}	4.52×10^{10}
3	$k_{\mathbf{SOS}}$	3.99×10^{10}	3.26×10^{10}	3.62×10^{10}

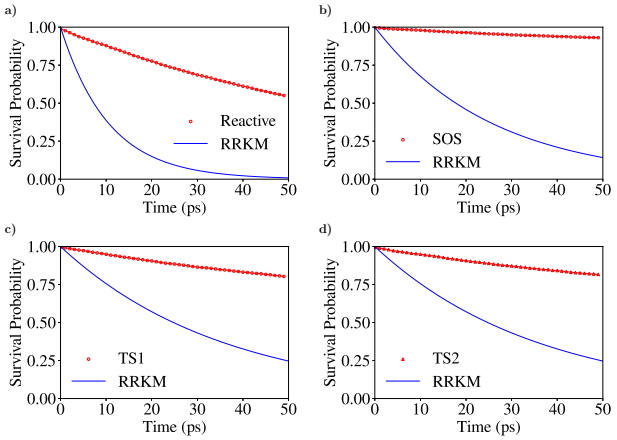

Figure 4. Comparison of survival probabilities (a) all reactive trajectories, trajectories reaching **PM** from (b) **SOS**, (c) **TS1**, and (d) **TS2** compared with their respective RRKM behaviour.

constant energy surface for guanidine molecule is 53 dimensional, it is not possible to study the entire phase space. Several studies have revealed that the non-linear frequencies associated with various modes can be extracted and the frequency ratios of relevant modes can shed light on the nature of the underlying high-dimensional phase space. This is done via partial mapping of the resonance network, also called Arnold web, in the phase space.[13–16] The general resonance condition for mode locking involving m oscillators can be written as,

$$\sum_{i}^{m} k_i \omega_i = 0 \tag{4}$$

where ω_i's are the frequencies of the oscillators and k_i's are integers.

Following the dynamics on a resonance network can give insights into important frequency lockings and local phase space structures that control the isomerization dynamics. However for a system like guanidine that has 21 vibrational modes, construction of a complete resonance network is not feasible. Dimensionality reduction techniques are the way

out to make the problem tractable, where one can understand the dynamics in terms of the most dominant atomic motions. We resorted to two methods of dimensionality reduction. In the first approach, by visualizing the IRC motions we identified three local coordinates that are important in the isomerization reaction - the angles ϕ and α defined above (Section 2) and the N−H stretching motion. In the second approach, we carried out principal component analysis (PCA) on the IRC in the Cartesian space, which can be considered to constitute the atomic motions connecting the various stationary points on the PES (details are given in Section S4). The first three components (PC1, PC2, and PC3) having the largest variances of 0.75, 0.14 and 0.05 primarily correspond to in-plane NH motion, out-of-plane NH motion and NH stretch respectively as has been reported in an earlier work by Rashmi et al., for MP2 dynamics of the same system.[19] The trajectories in Cartesian space were projected onto PC1, PC2, and PC3 to extract the dominant motions for further analysis.

Once the important coordinates and principal components were identified, the local frequencies associated with different motions from their time-series signals were extracted using the wavelet transform and the dynamical frequency ratio spaces were computed.[35,36] The details of the wavelet transform are mentioned in the SI (Section S5).

4.1. Local modes

For the local coordinates α, ϕ, and NH stretch, the resonance condition can be written as,

$$k_\alpha \omega_\alpha + k_{\mathrm{NH}} \omega_{\mathrm{NH}} + k_\phi \omega_\phi = 0 \tag{5}$$

Converting this equation in the form of a linear function results in a set of equations that give rise to a resonance network,

$$\frac{\omega_{\mathrm{NH}}}{\omega_\phi} = -\frac{k_\alpha}{k_{\mathrm{NH}}} \frac{\omega_\alpha}{\omega_\phi} - \frac{k_\phi}{k_{\mathrm{NH}}} \tag{6}$$

A static frequency ratio space or Arnold web corresponding to the energetically accessible region for guanidine isomerization formed by including all the resonances of order $\sum_j |k_j| \leq 7$ is shown in Figure 5.[37,38] This serves as a template for identifying resonance junctions in the FRS when the trajectories are propagated.

The time-evolved coordinates α, ϕ, and NH stretch extracted from the trajectories were subjected to wavelet transformation to obtain the time-dependent frequencies. The frequency ratios, $\omega_\alpha/\omega_\phi$ and $\omega_{\mathrm{NH}}/\omega_\phi$ for representative 400 reactive trajectories (200 via **SOS**, Path 1 + 200 via **TS2**, Path3) were calculated. Details of the method of wavelet transformation and the construction of FRS is described in the SI. Figure 6 shows the dynamical FRS constructed for **R→SOS→P** and **R→TS2→P** pathways. In general, the FRSs have similar characteristics for the trajectories following the **SOS** and **TS2** paths. The FRSs are anisotropic with localized patches of high densities. In other words, a large part the static web (Figure 5) is not accessed and only specific regions are visited in the dynamical web (Figure 6). This is an indication of underlying mixed phase space for the guanidine isomerization dynamics.[14–16] Four resonance junctions can be observed in each of the dynamical FRS considered here. The highest density was observed around $\omega_\alpha/\omega_\phi = 3/2$ and $\omega_{\mathrm{NH}}/\omega_\phi = 4$ (region A in FRS). The rest three resonance junctions with high densities are of higher orders.

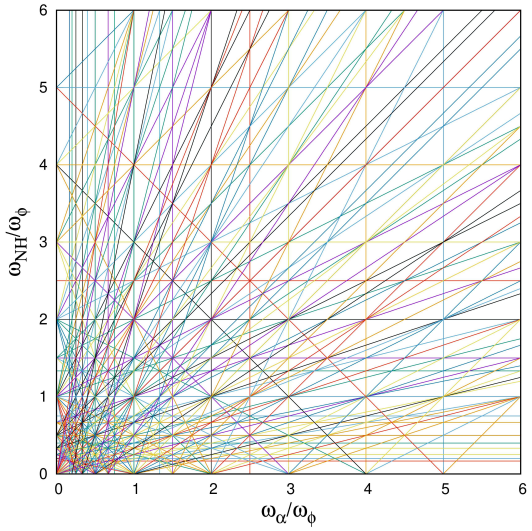

Figure 5. Static Arnold web of order 7 for the frequencies corresponding to $\omega_\phi, \omega_\alpha$ and ω_{NH}.

Further, in Figures 6(c) and 6(d), sample trajectories are shown (as black line) where the trajectories are seen traversing between various resonance zones. Thus, the enhanced density in the important resonance junctions could either come from frequent visits of every trajectory in the specific region of the FRS or from 'sticky' trajectories which upon entering the region could be trapped for a considerable time. Establishing whether these high-density regions are sticky is crucial since the existence of sticky regions in phase space imply long-time dynamical correlations which, in turn, have important implications for the transport mechanism. We checked for the stickiness of the regions by computing the residence times of trajectories in different regions of the FRS. Details about the calculation of the residence time is given in the SI. It can be seen that there are trajectories that have a residence time larger than 2 ps in a given region. Presence of such sticky trajectories in the phase space have been attributed to the origins of non-statistical reaction dynamics.[18]

4.2. Principal Components

The time-evolved Cartesian coordinates of the trajectories were projected onto the 3D PC space (PC1, PC2, PC3). The three PCs were then subjected to the wavelet-based time-frequency analysis. The frequency ratios, $\omega_{\mathrm{PC1}}/\omega_{\mathrm{PC2}}$ and $\omega_{\mathrm{PC3}}/\omega_{\mathrm{P2}}$ were obtained from the time-dependent frequencies associated with PC1, PC2, and PC3. The FRSs thus constructed in the PC space are shown in Figure S1 for representative trajectories following Paths 1 and 3. As seen in the FRS of local modes, Figure S1 clearly indicates the mixed nature of the underlying phase space with a dominant resonance junction at $\omega_{\mathrm{PC1}}/\omega_{\mathrm{PC2}} = 1.5$ and $\omega_{\mathrm{PC3}}/\omega_{\mathrm{PC2}} = 1.5$ along with several higher order resonances. Presence of these resonance junctions indicates the existence of regular dynamics and long-lived quasi-periodic trajectories in the phase space.[13,16]

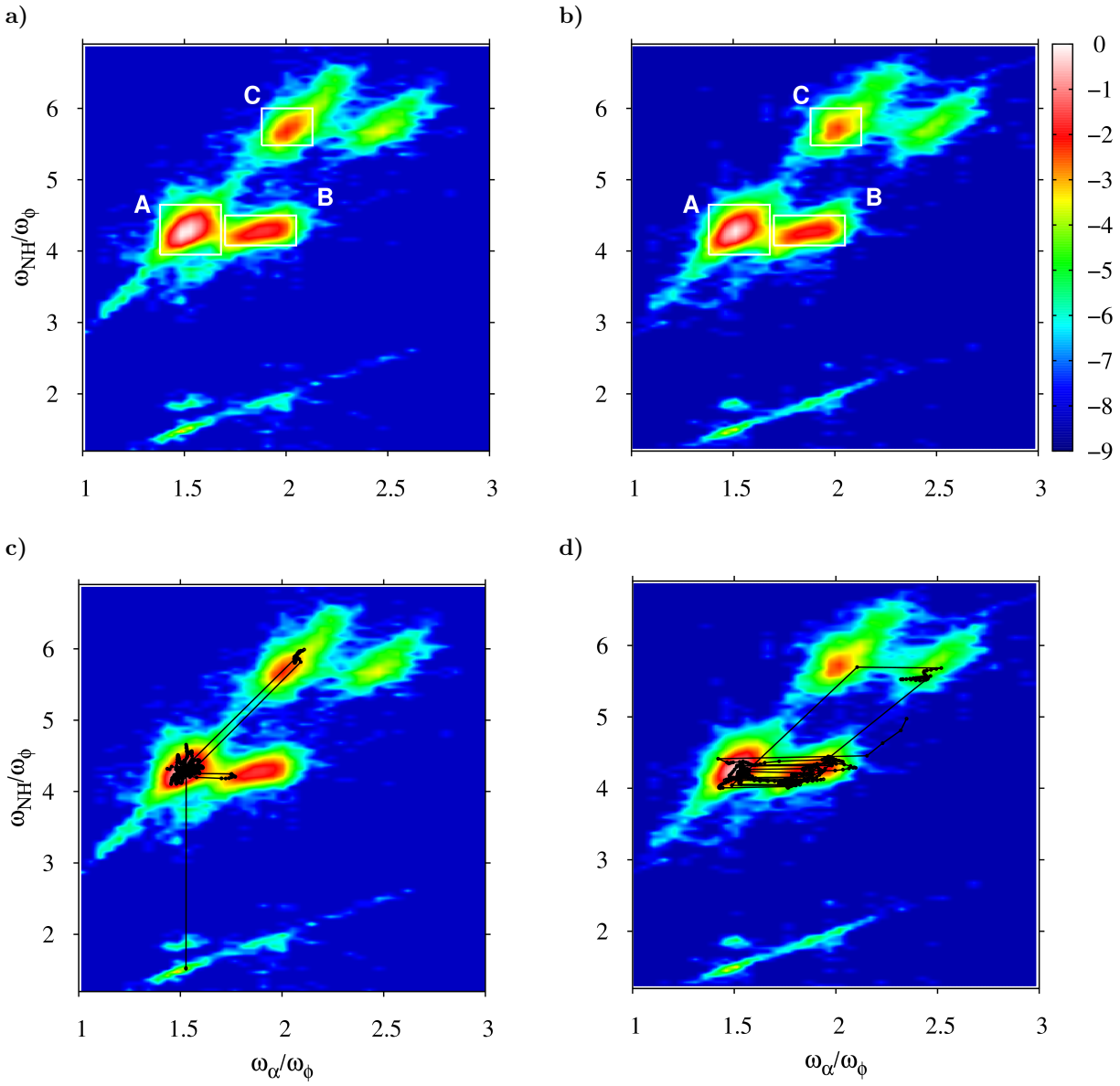

Figure 6. Local mode dynamical FRS between ω_{NH}/ω_ϕ and $\omega_\alpha/\omega_\phi$ for representative trajectories reaching **PM** from (a) **SOS** and (b) **TS2**. The high density regions are shown by boxes marked A, B and C for a closer look in terms of residence time distribution at those resonance junctions. Plot of representative trajectories following (c) **R→SOS→PW→PM** and (d) **R→TS2→PW→PM** pathways on their respective FRS that show hopping between several resonance junctions marked in the top panels. The densities are shown in logarithmic scale.

5. Conclusion

We have reported a semi-empirical trajectory study to understand the influence of second-order saddle in the dynamics of the *E-Z* isomerization in guanidine. The MEPs for the isomerization involve two transition states, **TS1** and **TS2** and an **SOS**. The dynamical simulations revealed a multitude of pathways followed by the different reactive trajectories. It was found that a higher fraction of trajectories reached the product minimum via the **TS1** or **TS2** and about 15% via the **SOS**. Many of these trajectories accessed multiple saddle points before forming the product. In addition, about 2% of the reactive trajectories showed recrossing events which is indicative of non-statistical dynamics. Survival probability distributions obtained from the dynamics exhibit large deviations from RRKM predictions further substantiating the presence of non-statistical dynamics. Time–frequency analysis coupled with dimensionality reduction methods were utilized to understand slow IVR and the nature of phase space transport. Comparison of the zeroth-order and the dynamical resonance networks indicate the anisotropic nature of the underlying classical phase space. In addition, the trajectories were found to have large residence times at the resonance junctions indicative of the stickiness in the dynamical frequency ratio space. We note that higher-dimensional barriers may exist in the phase space[39] in addition to the resonance junctions considered in the present work. Further, resonances involving only two modes were characterized in the present work. Multi-mode resonances[14] are also possible which were not investigated here.

Supplementary Information

Semi-empirical classical dynamics simulations, principal component analysis, wavelet analysis, comparison of harmonic frequencies computed at MNDO and MP2/6-31+G*.

Acknowledgements

The authors thank NISER Bhubaneswar for computational facilities. This work was supported by the grant of the Science and Engineering Research Board (SERB), India (No. EMR/2017/004843).

Conflict of Interest

The authors declare no conflict of interest.

Keywords: Guanidine • Frequency ratio space • Principal component analysis • Wavelet transformation • MNDO • Isomerization dynamics

References

[1] R. D. Levine, *Molecular reaction dynamics*, Cambridge University Press **2009**.
[2] W. Quapp, J. Maria Bofill, *Int. J. Quantum Chem.* **2015**, *115*, 1635.
[3] R. Minyaev, I. Getmanskii, W. Quapp, *Russ. J. Phys. Chem. C* **2004**, *78*, 1494.
[4] I. Getmanskii, R. Minyaev, *J. Struct. Chem.* **2008**, *49*, 973.
[5] Y. Harabuchi, Y. Ono, S. Maeda, T. Taketsugu, K. Keipert, M. S. Gordon, *J. Comput. Chem.* **2016**, *37*, 487.
[6] J. S. Chen, K. Houk, C. S. Foote, *J. Am. Chem. Soc.* **1998**, *120*, 12303.
[7] G. S. Ezra, S. Wiggins, *J. Phys. A* **2009**, *42*, 205101.
[8] P. Collins, G. S. Ezra, S. Wiggins, *J. Chem. Phys.* **2011**, *134*, 244105.
[9] R. Pradhan, U. Lourderaj, *Phys. Chem. Chem. Phys.* **2017**, *19*, 27468.
[10] R. Pradhan, U. Lourderaj, *Phys. Chem. Chem. Phys.* **2019**, *21*, 12837.
[11] K. Yadav, R. Pradhan, U. Lourderaj, *Faraday Discuss.* **2022**.
[12] P. Pandey, S. Naik, S. Keshavamurthy, *Regul. Chaotic Dyn.* **2021**, *26*, 165.
[13] C. C. Martens, M. J. Davis, G. S. Ezra, *Chem. Phys. Lett.* **1987**, *142*, 519.
[14] P. Manikandan, S. Keshavamurthy, *Proc. Natl. Acad. Sci.* **2014**, *111*, 14354.
[15] A. Sethi, S. Keshavamurthy, *Mol. Phys.* **2012**, *110*, 717.
[16] P. K. Yadav, S. Keshavamurthy, *Faraday Discuss.* **2015**, *177*, 21.
[17] S. Karmakar, P. K. Yadav, S. Keshavamurthy, *Commun. Chem.* **2020**, *3*, 1.
[18] S. Karmakar, S. Keshavamurthy, *Phys. Chem. Chem. Phys.* **2020**, *22*, 11139.
[19] R. Rashmi, K. Yadav, U. Lourderaj, M. Paranjothy, *Regul. Chaotic Dyn.* **2021**, *26*, 119.
[20] S. R. Hare, L. A. Bratholm, D. R. Glowacki, B. K. Carpenter, *Chem. Sci.* **2019**, *10*, 9954.
[21] T. Tsutsumi, Y. Ono, Z. Arai, T. Taketsugu, *J. Chem. Theory Comput.* **2020**, *16*, 4029.
[22] T. Tsutsumi, Y. Ono, T. Taketsugu, *Top Curr. Chem.* **2022**, *380*, 1.
[23] J. Stewart, L. Fiedler, J. Zheng, P. Zhang, I. Rossi, W. Hu, G. Lynch, Y. Liu, Y. Chuang, J. Pu, J. Li, C. Cramer, P. Fast, J. Gao, D. Truhlar **2015**, university of Minnesota, Minneapolis, MN 55455.
[24] W. L. Hase, R. J. Duchovic, X. Hu, A. Komornicki, K. F. Lim, D.-h. Lu, G. H. Peslherbe, K. N. Swamy, S. Linde, A. Varandas, et al., *QCPE Bull.* **1996**, *16*, 671.
[25] X. Hu, W. L. Hase, T. Pirraglia, *J. Comput. Chem.* **1991**, *12*, 1014.
[26] B. Jayee, W. L. Hase, *Annu. Rev. Phys. Chem.* **2020**, *71*, 289.
[27] S. Keshavamurthy, *Adv. Chem. Phys* **2013**, *153*, 43.
[28] D. J. Nesbitt, R. W. Field, *J. Phys. Chem.* **1996**, *100*, 12735.
[29] B. K. Carpenter, *Annu. Rev. Phys. Chem.* **2005**, *56*, 57.
[30] D. J. Tantillo, Beyond transition state theory – Nonstatistical dynamic effects for organic reactions, in *Advances in Physical Organic Chemistry*, volume 55, pages 1–16, Elsevier **2021**.
[31] L. Zhu, W. Hase, *QCPE Bull.* **1994**, *14*.
[32] P. Haarhoff, *Mol. Phys.* **1964**, *7*, 101.
[33] O. K. Rice, H. C. Ramsperger, *J. Am. Chem. Soc.* **1927**, *49*, 1617.
[34] R. A. Marcus, *J Chem. Phys.* **1952**, *20*, 359.
[35] L. V. Vela-Arevalo, S. Wiggins, *Int. J. Bifurc. Chaos* **2001**, *11*, 1359.
[36] C. Chandre, S. Wiggins, T. Uzer, *Phys. D: Nonlinear Phenom.* **2003**, *181*, 171.
[37] N. Guillery, J. D. Meiss, *Regul. Chaotic Dyn.* **2017**, *22*, 700.
[38] V. I. Arnol'd, *Russ. Math. Surv.* **1963**, *18*, 85.
[39] G. S. Ezra, H. Waalkens, S. Wiggins, *J. Chem. Phys.* **2009**, *130*, 164118.

Supplementary Information for: Non-statisticality in *E*-*Z* Isomerization Reaction of Guanidine: Second-order Saddle Dynamics and Time-frequency Analysis

Richa Rashmi,[+,a] Pankaj Kumar Yadav,[+,a] Aniruddha Seal,[a] Manikandan Paranjothy*[b] Upakarasamy Lourderaj,*[a]

[a]*School of Chemical Sciences, National Institute of Science Education and Research (NISER) Bhubaneswar, An OCC of Homi Bhabha National Institute, P.O. Jatni, Khurda, Odisha, India*

[b]*Department of Chemistry, Indian Institute of Technology Jodhpur, Jodhpur, Rajasthan, India*

Email: pmanikandan@iitj.ac.in, u.lourderaj@niser.ac.in

S1. Comparison of different semi-empirical methods

A comparison of the energies and imaginary frequencies of the stationary points (**TS2**, **SOS**) obtained using different semi-empirical methods for *E-Z* isomerization of guanidine is presented in Table S1.

Table S1: Energies and important mode frequencies obtained using different semi-empirical methods compared with that of MP2/6-31+G* level for guanidine isomerization

S. No.	**Method**	**Energy (kcal/mol)**		**Mode frequency (cm^{-1})**		
		TS2	**SOS**	**in-plane**	**out-of-plane**	**torsional**
1	MP2	23.67	24.65	$1078i$	$368i$	$1031i$
2	MNDO	26.84	27.40	$1210i$	$260i$	$1204i$
3	MINDO/3	-	12.56	$756i$	$392i$	-
4	RM1	-	17.72	$880i$	$405i$	-
5	RM1-D	-	17.92	$882i$	$414i$	-
6	AM1	-	23.35	$1121i$	$275i$	-
7	PM3	22.56	24.98	$1402i$	$475i$	$1194i$
8	PM3-D	20.60	23.70	$1403i$	$518i$	$1115i$
9	PM6	15.00	17.00	$1043i$	$407i$	$799i$
10	PM6-D	15.00	17.00	$1046i$	$416i$	$802i$

S2. Classification of Trajectory Pathways

S2.1. Stationary Point Regions

To understand the dynamical pathways followed in the reaction, different regions on the PES were identified as given below. A total of 1000 trajectories each were initialized in **TS1**, **TS2**, and **SOS** regions corresponding to $E_{\text{total}} = 77.81$ kcal/mol. The geometrical parameters α and ϕ obtained from the initial coordinates of these trajectories in each region were used to define the different saddle point regions in the configuration space. For example, to define the **TS2** region, the deviation of the α and ϕ values from the equilibrium values for **TS2** ($\Delta\alpha = \alpha - \alpha_0$ and $\Delta\phi = \phi - \phi_0$) were computed for the sampled initial coordinates. The initial coordinates for which $\Delta\alpha$ and $\Delta\phi$ were below the 98^{th} percentile were considered and the corresponding ranges in α and ϕ defined the **TS2** region.[1] The **PM** region is an area on the 2D PES about the **P** stationary point (*Z*-guanidine) within α and ϕ variation of up to 30°. The six stationary point regions (**R, TS1, TS2, SOS, PW, PM**) and a dividing surface thus identified on the 2D PES are given in Table S2 and shown in Figure 2 in the main text.

It should be noted that a trajectory, on crossing the dividing surface, enters the product well region (**PW**) and then either forms the product defined by the region around the product minimum (**PM**), or recrosses the dividing surface without reaching the **PM** region. Thus, the two regions **PW** and **PM** were differentiated to identify recrossing events.

Table S2: Regions defined on the PES to classify dynamical pathways followed by trajectories

S. No.	Stationary Point Region	Range for α	Range for ϕ
1	SOS	$\alpha \leq 11.43^\circ$	$0^\circ \leq \phi < 360^\circ$
2	TS1	$\alpha > 11.43^\circ$	$92.49^\circ \leq \phi \leq 115.25^\circ$
3	TS2	$\alpha > 11.43^\circ$	$260.14^\circ \leq \phi \leq 284.40^\circ$
4	R	$\alpha > 11.43^\circ$	$(284.40^\circ < \phi \leq 360^\circ) \cup (0^\circ \leq \phi < 92.49^\circ)$
5	PW	$\alpha > 11.43^\circ$	$115.25^\circ < \phi < 260.14^\circ$
6	PM	$34.4^\circ < \alpha < 94.4^\circ$	$155.8^\circ < \phi < 215.8^\circ$

S2.2. Pathways

The dynamical pathways followed by the trajectories were classified by tracking the regions accessed by them before forming the products. The trajectory pathways were found to be quite complex with several trajectories accessing multiple regions defined above before forming products. Thus, for simplicity, a trajectory pathway was labelled by tracing back the path from the product (**PM**) until it reaches the **R** region. For example, a trajectory following the path **R**→**TS2**→**R**→**TS1**→**R**→**SOS**→**PW**→**PM** is classified as **R**→**SOS**→**PW**→**PM** pathway.

S3. Comparison of MNDO frequencies with MP2/6-31+G*

The harmonic frequencies of the stationary points (**R**, **SOS**, **TS1**, **TS2**) optimized using semi-empirical Hamiltonian MNDO are compared with that computed at MP2/6-31+G* level of theory in Table S3.

S4. Principal Component Analysis

Principal Component Analysis (PCA) is one of the earliest and most widely used techniques to reduce the dimensionality of a high dimensional data. The primary purpose behind performing a PCA in the present work is to follow the dynamics of guanidine isomerization in a reduced-dimensional space. We use the implementation by Carpenter and coworkers[2] which involves the following sequence of steps:

1. IRC in Principle Components: We use a m × 3N dimensional matrix $\mathbf{X}$ constructed using m data points on the IRC in the Cartesian space as input. The data is centered along the mean $\overline{\mathbf{X}}$ and then transformed to a new orthogonal basis (principal components or PCs) $\mathbf{T}$ given by $\mathbf{T} = \overline{\mathbf{X}}\mathbf{W}$. The transformation matrix $\mathbf{W}$ is obtained by diagonalizing the covariance matrix $\mathbf{C} = \overline{\mathbf{X}}^{\mathrm{T}}\overline{\mathbf{X}}$

2. IRC in Reduced Dimensions: We reduce the dimensionality of our data by considering first k components having the largest variances. The reduced dimensional transformation is given by $\mathbf{T}_{\mathrm{k}} = \overline{\mathbf{X}}\mathbf{W}_{\mathrm{k}}$ where $\mathbf{T}_{\mathrm{k}}$ corresponds to first k PCs and $\mathbf{W}_{\mathrm{k}}$ is the reduced-dimensional transformation matrix.

3. Projection of Trajectory Data onto Reduced Dimensions: Each point on the trajectory is projected onto the IRC in the reduced-dimensional PC space.

Table S3: Comparison of harmonic frequencies of **R**, **TS1**, **TS2**, and **SOS** computed at MNDO and MP2/6-31+G*

S. No.	Reactant		SOS		TS2		TS1	
	MP2	MNDO	MP2	MNDO	MP2	MNDO	MP2	MNDO
1	367	167	$1078i$	$1210i$	$1031i$	$1204i$	$1031i$	$1203i$
2	414	234	$368i$	$260i$	331	239	330	239
3	484	493	387	185	471	256	470	257
4	540	528	440	253	483	418	483	418
5	611	606	495	483	507	509	507	509
6	708	823	556	541	548	529	548	529
7	795	939	614	611	596	612	595	612
8	847	1057	737	960	697	830	696	830
9	957	1144	785	989	757	908	757	908
10	1135	1269	942	1135	967	1142	967	1142
11	1151	1312	1072	1257	1060	1234	1060	1234
12	1219	1323	1234	1313	1217	1294	1217	1294
13	1482	1619	1372	1514	1397	1531	1397	1531
14	1675	1799	1679	1809	1666	1804	1666	1805
15	1693	1830	1684	1821	1680	1822	1680	1822
16	1771	1941	1865	2077	1789	1967	1789	1967
17	3513	3540	3561	3557	3569	3567	3569	3567
18	3562	3558	3564	3559	3581	3581	3581	3581
19	3566	3576	3686	3591	3699	3597	3698	3597
20	3677	3577	3687	3592	3712	3603	3712	3603
21	3682	3590	3945	3781	3828	3730	3829	3730

S5. Wavelet Analysis

To compute the local frequencies we use the wavelet-based time-frequency approach of Arevalo and Wiggins[3]. The local frequencies associated with a time-dependent function $f(t)$ can be obtained upon wavelet transform of the function as given below

$$L_g f(a,b) = \frac{1}{\sqrt{a}} \int_{-\infty}^{\infty} f(t) g\left(\frac{t-b}{a}\right) dt \tag{1}$$

where b and a are parameters controlling the translation and dilations of the mother wavelet. The mother wavelet used in this work is the Morlet-Grossman wavelet defined as

$$g(t) = \frac{1}{\sigma\sqrt{2\pi}} e^{2\pi i\lambda t} e^{-t^2/2\sigma^2} \tag{2}$$

where λ and σ are tuning parameters with values of 1 and 2, respectively. The wavelet transform gives the local frequency of $f(t)$ over a small interval of time around $t = b$ and inverse of the scale factor a is proportional to the frequency. A distinct advantage of the wavelet approach is that the time window automatically narrows for high frequency and vice versa. Therefore it keeps track of the rapid variation of the instantaneous frequencies. The value of the most dominant local frequency at a given time $t = b$ is extracted by determining the scale a which maximizes the modulus of the wavelet transform. In this way we get the spectral content of a trajectory over a small interval of time around $t = b$.

S6. Frequency ratio space

The frequency ratio space (FRS) was constructed by dividing the space into 120×120 cells and recording the total number of visitations in a particular cell by trajectories noted from their frequency ratio time-series. The procedure was repeated with 200 representative trajectories from each class of trajectories studied. The highest density was then normalized to one and plotted on the logarithmic scale in order to highlight the key regions in FRS.

The time-evolved Cartesian coordinates of the trajectories were projected onto the 3D PC space (PC1, PC2, PC3). The three PCs were then subjected to the wavelet-based time-frequency analysis. The frequency ratios, $\omega_{PC1}/\omega_{PC2}$ and ω_{PC3}/ω_{P2} were obtained from the time-dependent frequencies associated with PC1, PC2, and PC3 and the dynamical FRS constructed for trajectories reaching the product from **SOS** and **TS2** is shown in Figure S1 .

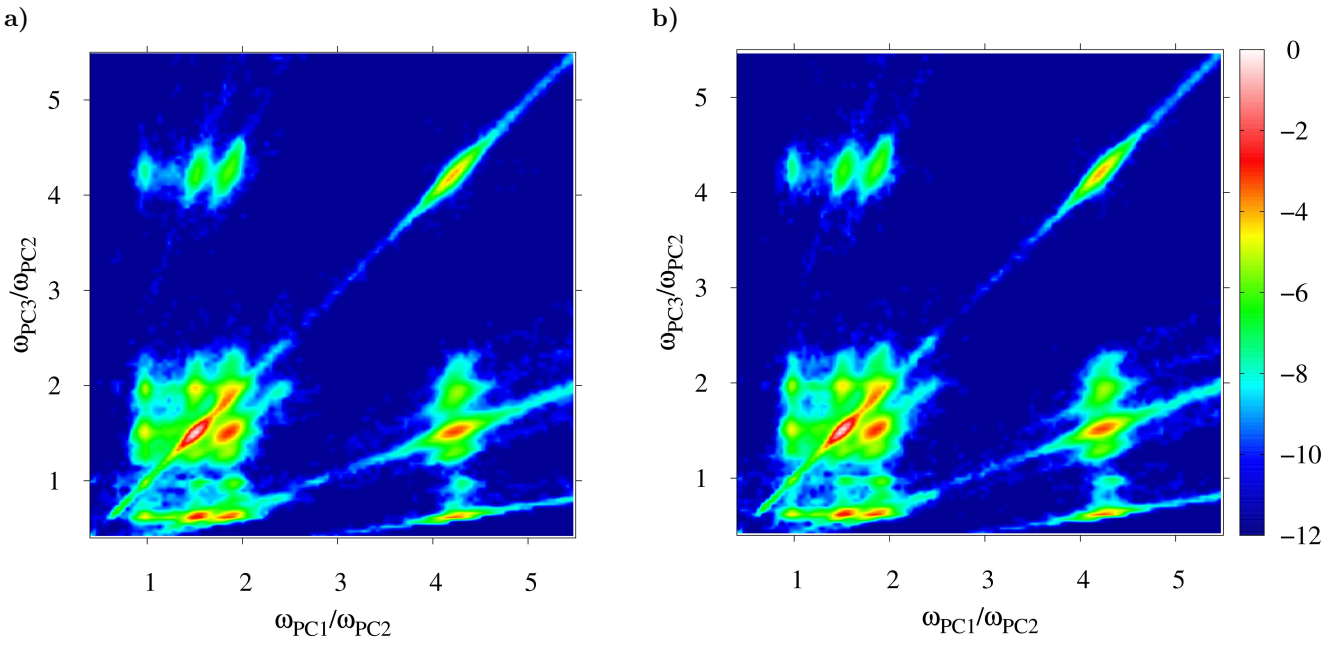

Figure S1: Principal component dynamical frequency ratio space for trajectories reaching **PM** from (a) **SOS** and (b) **TS2**.

S7. Residence Time

The residence time is defined as the longest time interval a trajectory spends within the boundary of the various cells in the FRS (see description of FRS). The residence time is defined as,

$$t_{res} = t_2 - t_1 \tag{3}$$

where t_1 is the time when a trajectory enters a cell and t_2 is the time when a trajectory leaves the cell. Here a trajectory can have multiple such events and from these locking events, we noted the longest locking time for a particular trajectory. In this fashion, we computed the longest residence time for all the trajectories and made the residence time distribution shown in Figure S2. We computed the residence time distribution at three high density resonance junctions on the local mode FRS (marked by boxes in Figure 6 in the main text).

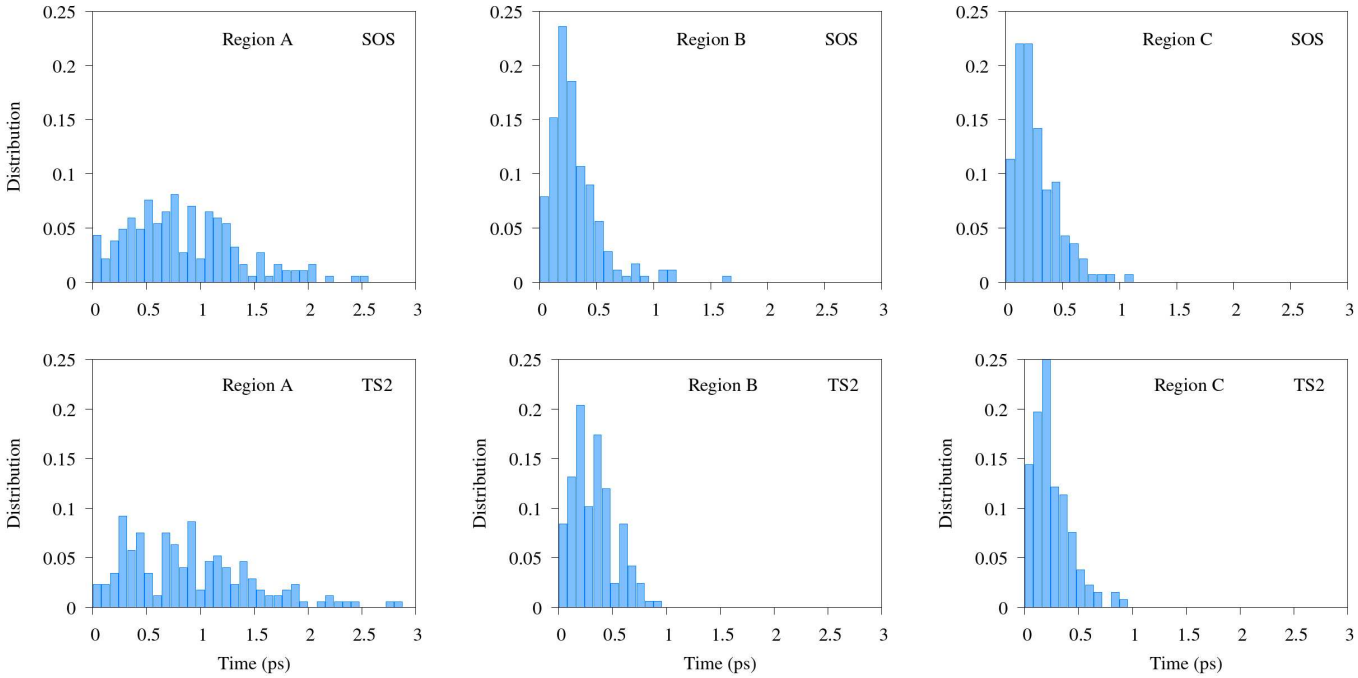

Figure S2: Longest residence time distribution computed from the local mode FRS in the high density resonance junctions A, B and C (enclosed by boxes in Figure 6 in the main text) for trajectories reaching **PM** from **SOS** (Top Panel) and **TS2** (Bottom Panel).

References

[1] K. Black, P. Liu, L. Xu, C. Doubleday and K. N. Houk, *Proc. Natl. Acad. Sci.*, 2012, **109**, 12860–12865.

[2] S. R. Hare, L. A. Bratholm, D. R. Glowacki and B. K. Carpenter, *Chem. Sci.*, 2019, **10**, 9954–9968.

[3] L. V. Vela-Arevalo and S. Wiggins, *Int. J. Bifurc. Chaos*, 2001, **11**, 1359–1380.